




Article

Innovative Magnetite Based Polymeric Nanocomposite for Simultaneous Removal of Methyl Orange and Hexavalent Chromium from Water

Norah Salem Alsaiari ¹, Abdelfattah Amari ^{2,3,*}, Khadijah Mohammedsaleh Katubi ^{1,*},
Fatimah Mohammed Alzahrani ^{1,*} , Faouzi Ben Rebah ^{4,5,*}  and Mohamed A. Tahoon ^{4,6} 

¹ Chemistry Department, College of Science, Princess Nourah Bint Abdulrahman University, Riyadh 11671, Saudi Arabia; nsalsaiari@pnu.edu.sa

² Department of Chemical Engineering, College of Engineering, King Khalid University, P.O. Box 9004, Abha 61413, Saudi Arabia

³ Research Laboratory: Energy and Environment, Chemical Engineering Department, National School of Engineers, Gabes University, Gabes 6072, Tunisia

⁴ Department of Chemistry, College of Science, King Khalid University, P.O. Box 9004, Abha 61413, Saudi Arabia; tahoon_87@yahoo.com

⁵ Higher Institute of Biotechnology of Sfax (ISBS), Sfax University, P.O. Box 263, Sfax 3000, Tunisia

⁶ Chemistry Department, Faculty of Science, Mansoura University, Mansoura 35516, Egypt

* Correspondence: abdefattah.amari@enig.rnu.tn (A.A.); kmkatubi@pnu.edu.sa (K.M.K.); fmalzahrani@pnu.edu.sa (F.M.A.); benrebahf@yahoo.fr (F.B.R.)



Citation: Alsaiari, N.S.; Amari, A.; Katubi, K.M.; Alzahrani, F.M.; Rebah, F.B.; Tahoon, M.A. Innovative Magnetite Based Polymeric Nanocomposite for Simultaneous Removal of Methyl Orange and Hexavalent Chromium from Water. *Processes* **2021**, *9*, 576. <https://doi.org/10.3390/pr9040576>

Academic Editor: Katherine M. E. Stewart

Received: 27 February 2021

Accepted: 24 March 2021

Published: 26 March 2021

Publisher's Note: MDPI stays neutral with regard to jurisdictional claims in published maps and institutional affiliations.



Copyright: © 2021 by the authors. Licensee MDPI, Basel, Switzerland. This article is an open access article distributed under the terms and conditions of the Creative Commons Attribution (CC BY) license (<https://creativecommons.org/licenses/by/4.0/>).

Abstract: One of the most important directions for environmental remediation is the effective removal of dyes and toxic heavy metals from water using newly fabricated nano-adsorbents. Here, magnetic Fe₃O₄ nanoparticles were combined with nitrogen-containing functional group polymers chitosan (CS) and polypyrrole (ppy) to synthesize a nanocomposite (polypyrrole@magnetic chitosan) useful for removing methyl orange (MO) and hexavalent chromium (Cr (VI)) from water. The physicochemical properties of the nanocomposite were determined using SEM, TEM, XRD, FT-IR, and TGA techniques. The effect of different factors on the adsorption system was studied including the contact time, pH, and the effect of co-existed ions. The kinetic study illustrated that the adsorption fit well with Langmuir isotherm. The maximum adsorption capacity of MO and Cr (VI) was found to be 95 and 105 mg/g, respectively. The reusability of the nanocomposite was studied for up to five cycles using 0.1 M NaOH as eluent with a slight decrease of adsorbent efficiency. Furthermore, the removal mechanism studied suggested the removal of MO via adsorption and Cr (VI) via chemical reduction and adsorption. This study suggests that a ppy@magnetic chitosan nanocomposite is a promising nano-adsorbent for removing MO and Cr (VI) from water.

Keywords: environment; polymers; nanomaterials; water treatment

1. Introduction

Environmental degradation and the lack of clean water have become universal problems associated with the fast increase in industrial activity and social economy and should be solved to maintain a high-quality life [1–3]. Recently, great attention has been paid to water treatment for heavy metals [4,5] resulting from steel fabrication, leather tanning, and metal processing and from toxic dyes from the paper, cosmetics, plastics, textile, and food industries. Among these pollutants, the organic dye methyl orange (MO) can cause severe health problems like jaundice, tissue necrosis, tachycardia, vomiting, and cyanosis. Furthermore, as a conventional toxic heavy metal, chromium not only causes significant damage to human health, but also generates extreme environmental contamination that is hard to remediate [6]. Trivalent chromium Cr (III) and hexavalent chromium Cr (VI) are the two oxidation states of chromium [7]. Cr (VI) is carcinogenic and known to be a very

dangerous contaminant, while Cr (III) is less toxic to humans and other organisms and is less movable in environmental systems [8]. According to the World Health Organization (WHO), the allowable level of Cr (VI) in water must not exceed 0.05 mg/L [9]. However, in wastewater from chromium electroplating, the Cr (VI) levels were found to reach 100 to 500 mg/L. Thus, the transformation of Cr (VI) to Cr (III) via an efficient reduction concept and the efficient adsorption of MO can greatly decrease the possible hazard of Cr (VI) and MO dye to animals, humans, and the environment [10,11]. Water contamination from chromium and dye has been widely remediated over the past years. In this context, Cr (VI) and MO have been efficiently removed using various techniques including adsorption, electrochemical methods, reduction, biological remediation, ion exchange, and chemical precipitation [12–15]. Due to its low cost, great efficiency, and simple processing procedures, adsorption is considered the most promising method. Several adsorbents have been proposed for the effective removal of MO and Cr (VI): carbon nanomaterials [16,17], layered double hydroxides [18,19], agricultural waste [16], chitosan [20], metal oxides [21], zeolites [22], and clay minerals [23]. The biocompatibility, nontoxicity, and biodegradability of chitosan make it attractive among other materials for removing of pollutants from water. Chitosan is a polysaccharide with a linear structure resulting from the alkaline treatment of the second-most abundant biopolymer in nature (chitin), which is present in the shells of lobsters, crabs and shrimp [24]. Chitosan is bio-attracted to negatively charged moieties and is water soluble because of an amino group that has a pKa of 6.5, causing it to be easily protonated in a neutral medium and acidic solution. Its molecular structure has large numbers of hydroxyl and amino groups that provide chelation power toward different metal ions [25]. Although adsorption is the most efficient method for Cr (VI) and MO removal, it is considered to be nondestructive, and the regeneration of the adsorbed materials limits the application of chitosan to treat real wastewater. Additionally, only the phase transition of contaminants can be realized by adsorption alone although their intrinsic essence (physicochemical property and toxicity) remains unchanged. Therefore, the best solution is to fabricate a material that can provide in situ chemical reduction of Cr (VI) to Cr (III) (considered less toxic with useful characteristics for organisms) and the simultaneous adsorption of both MO and Cr (VI); however, the association of reduction removal with adsorption has rarely been studied. Moreover, the common recovery techniques used for adsorption—centrifugation, sedimentation, and filtration—have several problems, including cost, high energy consumption, and low potency. The continued recycling of chitosan powder may not be easy due to its biodegradability; however, its adsorption ability has been improved using nanotechnology, which allows the incorporation of nanomaterials in the adsorbent material providing very small particle size and large surface area. However, these types of nanoadsorbents still suffer from decreased recycling performance and a complex separation process. Lately, as an adsorbent and adsorbent carrier, magnetic nanoparticles have shown exceptional properties such as simple chemical modification, a large specific surface area, and excellent magnetic characteristics and have attracted the attention of environmental engineers [26,27]. However, the lack of functional groups and the agglomeration of magnetic nanoparticles reduce their adsorption of pollutants. Accordingly, the development of a novel recyclable material having a high adsorption ability necessitates combining the benefits of polymer materials and magnetic nanoparticles (NPs). In recent years great attention has definitely been paid to magnetic chitosan nanocomposites constructed with a magnetic core of hematite (Fe_3O_4) NPs and a chitosan shell [28]. The fast and easy separation of an adsorbent by a commercial magnet as well as excellent mechanical features were provided via the combination of both magnetic NPs and a chitosan biopolymer. Furthermore, the adsorption capacity of magnetic chitosan can be increased by surface modification through the existing amino and hydroxyl groups on its surface. As previously reported, the modification of chitosan with different organic functional moieties (xanthate, α -ketoglutaric acid, thiourea, and ethylenediamine) could enhance its adsorption capacity toward different pollutants [29]. The low synthesis cost, biocompatibility, and better environmental stability enhanced the

application of a polypyrrole (Ppy)-conducting polymer for heavy metal removal from water [30]. Polypyrrole is a polymer with a molecular structure containing high numbers of imine groups that provide adsorption sites toward different dyes and metals. In addition to that, the imine groups provide a reduction capacity to convert Cr (VI) to Cr (III). Thus, Ppy can remove hexavalent chromium ions from water via both reduction and adsorption, and remove MO via adsorption. Based on this information, the in situ chemical reduction of Cr (VI) and the simultaneous adsorption of both Cr (VI) and MO could enhance the adsorption capacity. Interestingly, excellent separation ability could be obtained by fabricating a novel nanocomposite containing the three parts to exploit the advantages offered by each component: (i) reductant and adsorbent ability of polypyrrole; (ii) large number of hydroxyl and amino groups of chitosan; and (iii) magnetic characteristics of hematite nanoparticles (Fe_3O_4). As far as we know, there is no similar study. In particular, this novel nanocomposite detoxified water of both hexavalent chromium Cr (VI) and MO. Herein, the novel nanocomposite was synthesized via the combination of CS, Fe_3O_4 NPs, and polypyrrole. First, a one-step co-precipitation method was used to synthesize magnetic chitosan by mixing two oxidation states of iron with chitosan followed by the modification of magnetic chitosan with polypyrrole using oxidative polymerization to produce the nanocomposite ppy@CS/ Fe_3O_4 . This nanocomposite was tested to remove MO and Cr (VI) from water. The chemical composition, surface structure, and morphology of synthesized ppy@CS/ Fe_3O_4 were characterized via XRD, FT-IR, SEM, and TEM. In order to understand the removal mechanism, the effect of different factors on adsorption behavior (contact time, initial concentration, and pH) was studied. Lastly, the ppy@CS/ Fe_3O_4 nanocomposite was found to remove Cr (VI) via in situ chemical reduction and adsorption while MO was also adsorbed. This nanocomposite was found to be very promising for removing metals and dyes from water as shown by its recyclability and the stability of the obtained data.

2. Materials and Methods

2.1. Chemicals

Chitosan was used as received (Winlab Company, Leicester, UK, molecular weight = 100,000–300,000) while polypyrrole and pyrrole (98.0%) were supplied from Sigma-Aldrich (St. Louis, MO, USA). Sodium sulfate (99.0%), sodium chloride (99.9%), sodium bicarbonate (99.0%), hydrochloric acid (35.0%), sodium hydroxide pellets (97.0%), methyl orange (95.0%) and potassium dichromate (99.9%) were supplied from CDH chemicals (New Delhi, India), while ammonium persulfate, ferrous sulfate heptahydrate, and ferric chloride hexahydrate were supplied from Sinopharm Chemical Reagent Co., Ltd (Shanghai, China). All chemicals were of analytical grade and used without any additional purifications. Distilled water was used for the preparation of all experimental solutions.

2.2. Polypyrrole Magnetic Chitosan Synthesis

Firstly, the magnetic chitosan was prepared via the co-precipitation method as described in our previous work [31]. Briefly, two oxidation states of iron (FeCl_3 and FeSO_4 solutions) were mixed in a conical flask in 2:1 molar ratios, respectively, followed by the dropwise addition of aqueous ammonia (33%, *v/v*) accompanied by vigorous stirring under a nitrogen atmosphere for 30 min. After that, the nanoparticles were washed four times with distilled H_2O and collected with a permanent magnet. Then, a reverse-phase suspension method was used for the synthesis of magnetic chitosan in which a mixture of 0.6 mL of tween 80, 54 mL of mineral oil, and 200 mg of synthesized Fe_3O_4 NPs) was supplemented with 1% (*w/v*) of chitosan dissolved in an acetic acid solution. For 40 min, the resulting magnetic chitosan was stirred and sonicated followed by the addition of (4 mL, 25% *w/v*) glutaraldehyde. Stirring continued up to 5 h. Then, a permanent magnet was used to separate the synthesized magnetic chitosan, which was washed several times with acetone followed by drying at 45 °C in a vacuum. Secondly, the synthesized magnetic chitosan was modified using pyrrole monomers according the oxidative polymerization method, and 0.6 g of magnetic chitosan was added to 100 mL of water. Then, 2.5 mL

of pyrrole was added to the previous mixture followed by the addition of (5.0 mL, 1M) HCl solution. For 30 min, this mixture was stirred in an ice bath. An aqueous solution of ammonium persulfate (4 g in 20 mL) as initiator, was added to the mixture and stirred vigorously for four hours in an ice bath. Then, to 100 mL aqueous ammonia (33%, *v/v*) the recovered nanoparticles were added under continuous stirring for 13 h. Then, the product was washed several times with distilled water and ethyl alcohol followed by separation with a magnet and dried for 13 h at 75 °C.

2.3. Nanocomposite Characterization

The synthesized ppy@magnetic chitosan nanocomposite was characterized using different instruments including a UV/vis spectrometer, Raman spectrometer, magnetometer, thermogravimetric analysis (TGA) measurement, Fourier transform infrared (FT-IR) spectrophotometer, X-ray diffraction (XRD), scanning electron microscope (SEM), and transmission electron microscope (TEM). A UV spectrometer (UVD-2960, Labomed Inc., Los Angeles, CA, USA) was used to measure UV-visible absorption spectra. A triple Raman spectrometer (Horiba, Horiba Inc., Ann Arbor, MI, USA) was used to measure Raman spectra. A vibrating sample magnetometer (Lake Shore 7410, Lake Shore Cryotronics Inc., Westerville, OH, USA) was used to measure the magnetization of the nanocomposite. A Perkin Elmer, STA 6000 (PerkinElmer Inc., Shelton, CT, USA) was used to perform the thermogravimetric analysis in the temperature range of 30–800 °C with 30 °C min⁻¹ of heating rate under a nitrogen atmosphere. A Bruker, Tensor 27 FT-IR (Karlsruhe, Germany) spectrophotometer was used to perform FT-IR spectra in the range of 400–4000 cm⁻¹ at room temperature and collected at a resolution of 4 cm⁻¹. A GNR APD-2000 PRO (GNR, Cairo, Egypt) diffractometer was used to measure XRD using Cu K α radiation ($\lambda = 1.5406 \text{ \AA}$) operated at 45 kV. The diffraction intensities were recorded over the 2θ ranging from 5 to 90° with the constant scanning rate of 1°·min⁻¹. A TEM (JEM-2100F, Hillsboro, OR, USA) operating at 200 kV and a SEM (Hitachi S4800, Hitachi, Tokyo, Japan) were used, respectively, to study the size and morphology of the nanocomposite.

2.4. Adsorption Batch Experiments

A stock solution (1.0 g/L) of MO and dichromate salt (K₂Cr₂O₇) were prepared in distilled water and used for further dilution. For the study of the effectiveness of ppy@magnetic chitosan for removing MO and Cr (VI), adsorbent experiments were conducted in batch mode using 100 mL bottles. In each batch, 100 mg of the adsorbent (ppy@magnetic chitosan) was added to 50 mL of the pollutant solution (100 mg/L). The pH was adjusted using 1.0 M of HCl and 1.0 M of NaOH. Then, the samples were incubated under shaking (200 rpm at 25 °C) using a thermostated shaker. A permanent magnet was used to recover the adsorbent at certain intervals. The remaining supernatant was analyzed for MO and Cr (VI) residual concentrations using a UV-Vis spectrophotometer at λ_{max} of 465 and 541 nm, respectively. The effect of different parameters on adsorption performance (pH, contact times, and competing ions Cl⁻, HCO₃⁻, and SO₄²⁻) was studied. The recyclability of the adsorbent was also studied by immersing it after the experiment in 1.0 M NaOH as eluent (for one hour) then shaking it for 13 h. To examine the ppy@magnetic chitosan stability, the recovered adsorbent (with a magnet) was washed with water and ethyl alcohol four times, and then vacuum dried at 75 °C for 1 day. All adsorption experiments were performed in triplicate. The removal percentage (%) and adsorption capacity (mg/g) were determined according to the following equation:

$$\text{Adsorption capacity (mg/g)} = ((C_i - C_t)/m) \times V \quad (1)$$

Each symbol of the above two equations has a well-known meaning. V denotes the volume of solution, m denotes the mass of ppy@magnetic chitosan, and C_i and C_t represent the initial and final concentration of MO and Cr (VI) pollutants, respectively.

3. Results and Discussions

3.1. Nanocomposite Characterization

The morphology, size, and shape of synthesized magnetic chitosan and ppy@magnetic chitosan were characterized using SEM and TEM images as shown in Figure 1. According to Figure 1a, the SEM image of magnetic chitosan indicated the presence of abundant pores with rough surfaces. The surfaces of the material showed the presence of several spherical particles of about 26 nm that represent the magnetite nanoparticles (Fe_3O_4), thus signifying their effective construction in the fabricated composite.

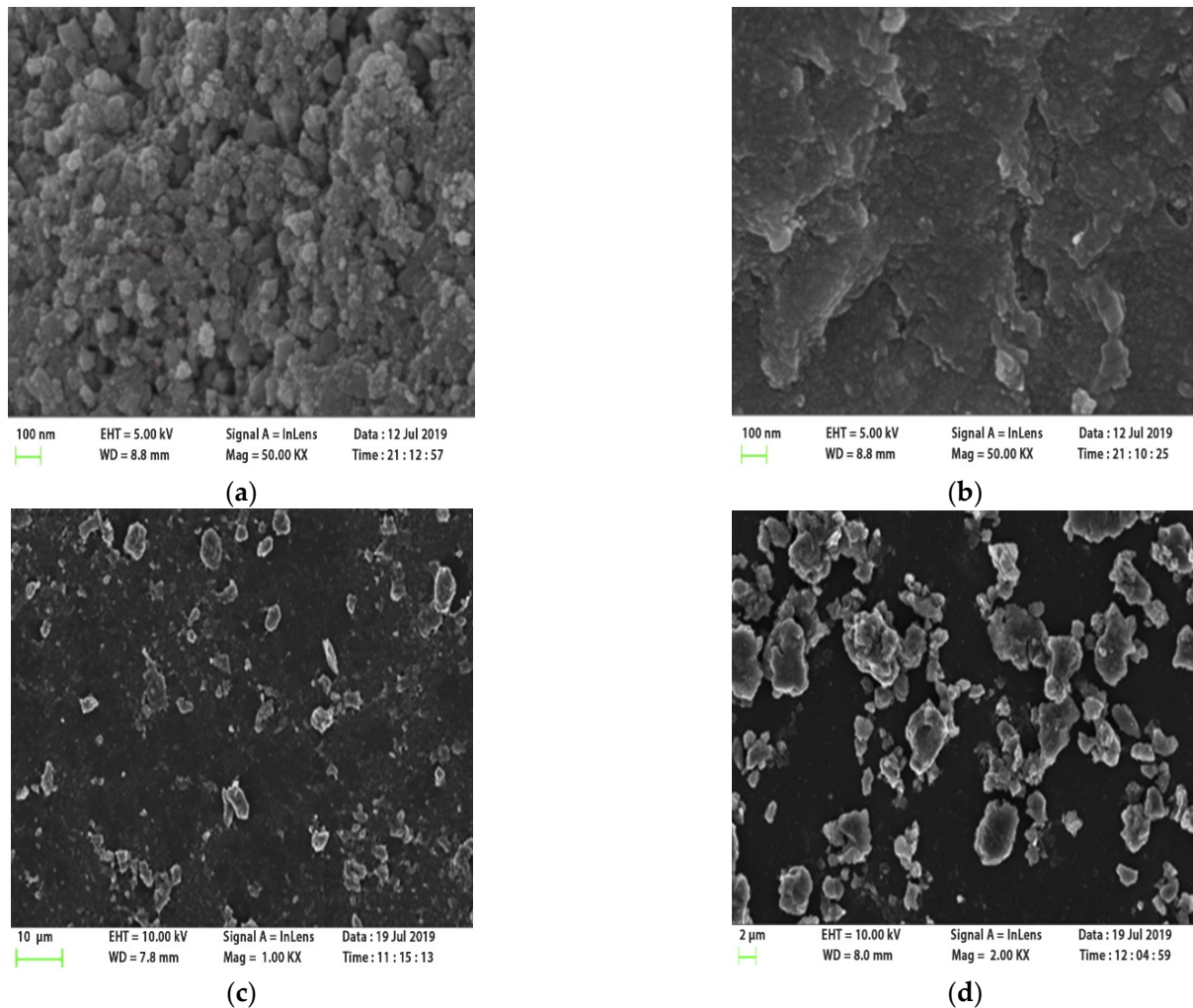


Figure 1. SEM image of (a) magnetic chitosan and (b) ppy@magnetic chitosan; TEM image of (c) magnetic chitosan and (d) ppy@magnetic chitosan (EHT: electron high tension, WD: working distance).

As observed, there was no clear aggregation phenomenon to indicate the excellent distribution of magnetite nanoparticles over the surface of composite. According to Figure 1b, the ppy loading over magnetic chitosan for the synthesis of the ppy@magnetic chitosan nanocomposite provided a smoother surface compared to that of magnetic chitosan. Polypyrrole was successfully loaded over the magnetic chitosan, which clearly indicated the presence of coated Fe_3O_4 nanoparticles, which were mainly implanted between the chitosan and polypyrrole (in the interior of the formed ppy@magnetic chitosan nanocomposite). According to Figure 1c,d, the ppy@magnetic chitosan nanocomposite and magnetic chitosan showed granular and irregular particles, respectively, with a size of 1.00–10.00 μm.

Polypyrrole, chitosan, and polypyrrole@magnetic chitosan nanocomposite XRD are shown in Figure 2a. Data for chitosan and polypyrrole were used for comparison. The amorphous structure of ppy was indicated from the wide peak observed at $2\theta = 22.85$ [32]. The two peaks of chitosan at $2\theta = 20.35$ and 9.95 are characteristic of the biopolymer chitosan. The definite regularity in the chitosan structure was attributed to the strong intra-inter-molecular hydrogen bonds formed by the plentiful amount of amino and hydroxyl groups in the chitosan structure [33]. Many diffraction peaks were present in the XRD of ppy@magnetic chitosan nanocomposite (as shown in Figure 2a) representing the planes (533), (620), (440), (511), (422), (400), (311), (220), and (111) of crystalline magnetite [34–36]. The small crystalline size of magnetite nanoparticles is indicated by very wide peaks compared to the bulk one. Using the Scherrer equation, the average crystalline size of the magnetite nanoparticles was found to be 10 nm by selecting the highest peaks for calculation. FT-IR spectroscopy was further used to characterize the synthesized ppy@magnetic chitosan nanocomposite as shown in Figure 2b. The broad peak of ppy@magnetic chitosan nanocomposite at 3357 cm^{-1} corresponds to the chitosan O–H axial stretching vibration band (3435 cm^{-1}) and ppy N–H stretching vibration band (3450 cm^{-1}), which are shifted in the spectrum of the nanocomposite. Also, the shift of the ppy peak at 1548 cm^{-1} to 1559 cm^{-1} in the synthesized nanocomposite as well as the disappearance of the chitosan peak at 1645 cm^{-1} indicated the strong interaction of both chitosan and ppy with the magnetite nanoparticles. The peaks at 1465 and 1559 cm^{-1} indicated the strong interaction and coating of chitosan and polypyrrole over the magnetite nanoparticles. The appearance of the new band at 571 cm^{-1} indicates the presence of magnetite as this band is characteristic of magnetite. The strong electrostatic interaction between NH_4^+ groups in both polymers (chitosan and ppy) and the negatively charged magnetite surface was indicated from the shift of the Fe–O bond peak at 581 and 585 cm^{-1} , which is characteristic of magnetite (571 cm^{-1}). FT-IR results indicate the good integration of chitosan, ppy, and Fe_3O_4 nanoparticles in the fabricated ppy@magnetic chitosan nanocomposite.

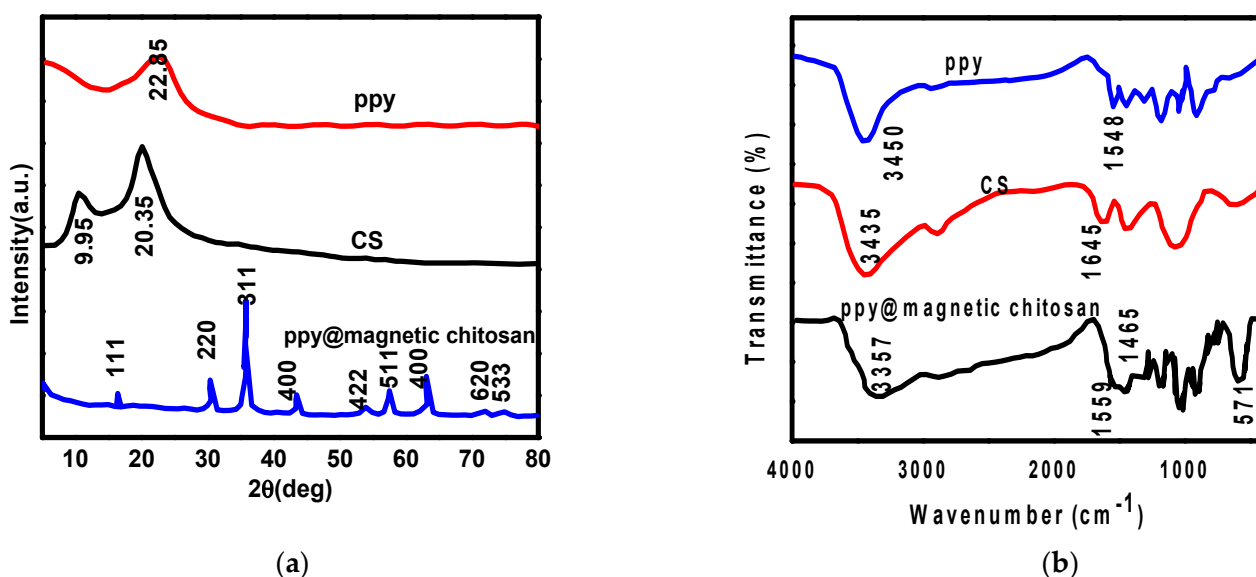


Figure 2. (a) XRD and (b) FT-IR of polypyrrole (ppy), chitosan (CS), and polypyrrole@magnetic chitosan nanocomposite (ppy@magnetic chitosan).

Raman spectroscopy was used to confirm integration among the three components of the nanocomposite as shown in Figure 3a. The observed two bands at 450 and 625 cm^{-1} are characteristic of Fe_3O_4 and were shifted from 533 and 669 cm^{-1} , respectively.

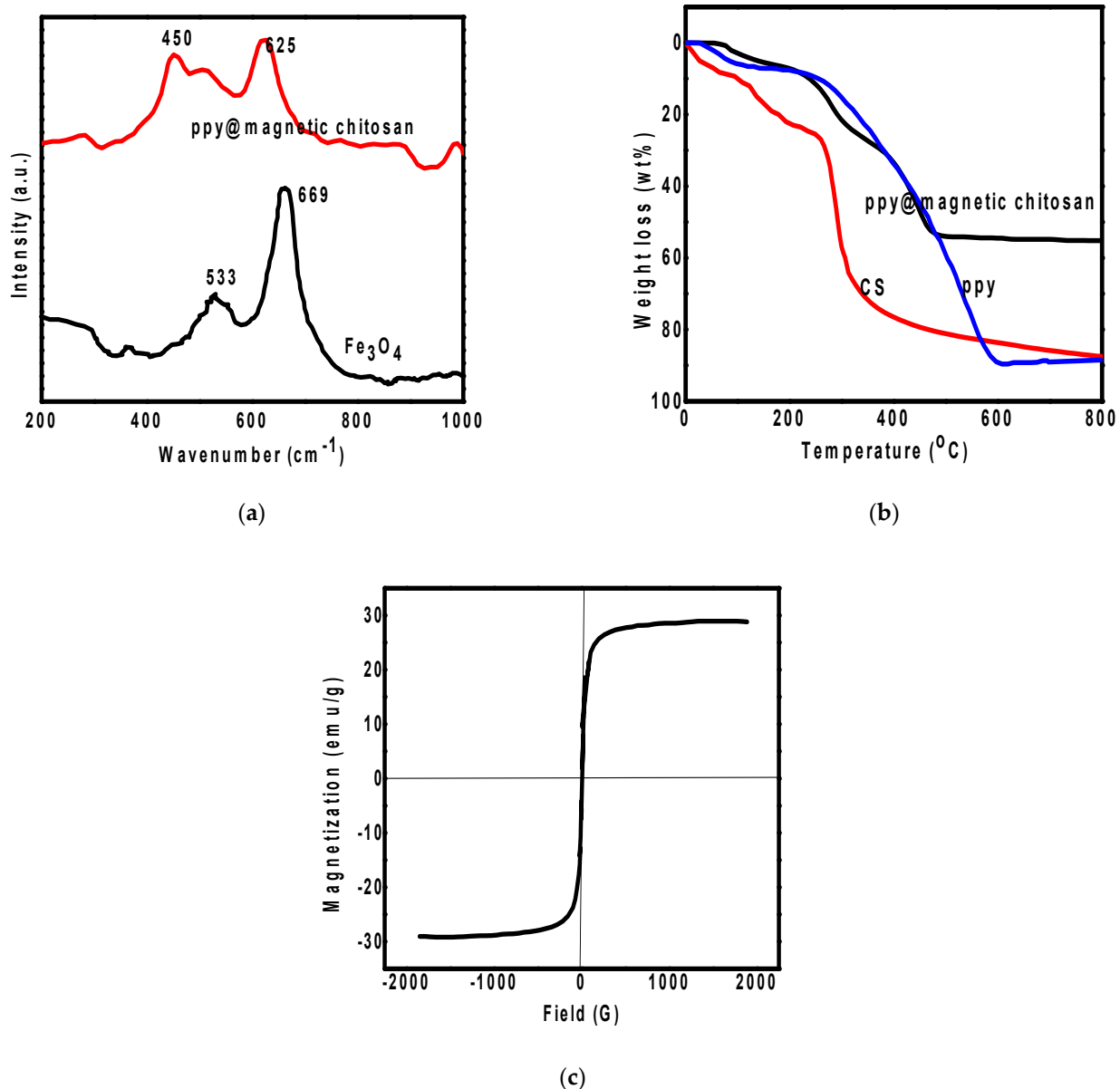


Figure 3. (a) Raman spectrum, (b) Thermogravimetric analysis, and (c) room temperature magnetization curve of polypyrrole@magnetic chitosan nanocomposite.

This Raman shift was an additional indicator of the strong interaction between the functional groups of chitosan and ppy polymers with the surface of Fe_3O_4 nanoparticles. For further data about the synthesized nanocomposite, the TGA investigation was achieved under N_2 atmosphere to obtain the thermal properties of the polypyrrole@magnetic chitosan nanocomposite as shown in Figure 3b, which shows three weight loss steps. Firstly, the weight loss between 41 and 166 °C corresponds to moisture loss from the polymer ppy. Secondly, the weight loss between 166 and 318 °C corresponds to the chitosan degradation. The last weight loss, between 318 and 489 °C, corresponds to the ppy main-chain degradation. One of the main advantages of the synthesized polypyrrole@magnetic chitosan nanocomposite is its simple separation from the medium by using a magnet. The magnetic properties of the nanocomposite were studied and provided in Figure 3c, which shows the relation between the applied field at room temperature and the magnetization of the studied nanocomposite. According to the magnetization curve, the lack of a hysteresis loop (H_c equal 0) indicates a superparamagnetic nature with no permanent magnetic moment. The high magnetic saturation moment (M_s) of polypyrrole@magnetic chitosan nanocomposite

(equal to 28.99 emu/g) was attributed to the magnetic Fe_3O_4 great loading. Due to its simple separation from medium solutions using external magnet, the superparamagnetic nanocomposite has attracted great attention for its application in water treatment. All the above characterization results approved the good integration and construction among the three parts of the polypyrrole@magnetic chitosan nanocomposite.

3.2. pH Effect on the Adsorption

The adsorbent active binding sites and surface chemistry are greatly influenced by the pH, which affects adsorption efficiency. Herein, we study the pH effect on MO, and Cr (VI) adsorption using polypyrrole@magnetic chitosan nanocomposite over a wide pH range from 2 to 12. Figure 4a illustrates the results. %clearpage

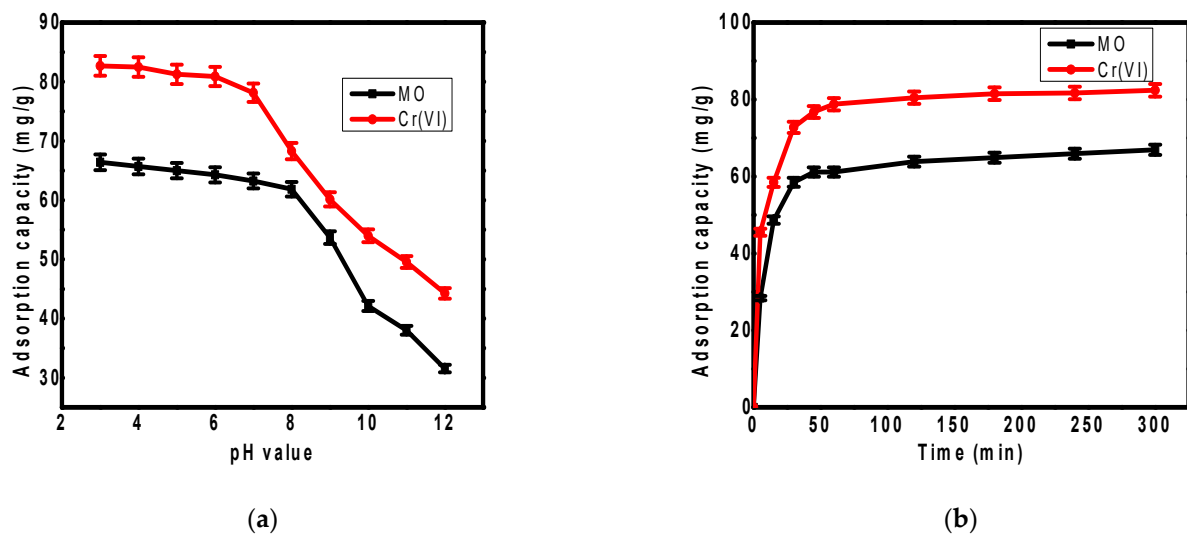


Figure 4. The effect of (a) pH value and (b) the contact time on the adsorption of MO and Cr (VI) over polypyrrole@magnetic chitosan nanocomposite.

The adsorption investigations to study the pH effect were performed at 25 °C with a contact time of 40 min, adsorbent dosage of 100 mg, initial concentration of both pollutants of 100 mg/L, and shaking rate of 200 rpm. The results showed that the removal of both Cr (VI) and MO are pH dependent. The pH increase led to a decrease in MO and Cr (VI) removal capacity due to the strong electrostatic interaction between the adsorbent positive charge at low pH and pollutants negative charge [37]. Additionally, at pH below 4.5, a high MO concentration could precipitate [38]. For Cr (VI), HCrO_4^- is the dominant anion at pH lower than 6 while at pH higher than 6 the dominant form is CrO_2^{4-} that cause electrostatic repulsion between different ions. Thus, at high pH the major reason for the decreased adsorption efficiency of MO and Cr (VI) was electrostatic repulsion. Consequently, the removal of MO and Cr (VI) over a polypyrrole@magnetic chitosan nanocomposite is very suitable in a neutral or acidic medium at an optimal pH value between 2 and 4.5. This behavior concerning the removal of both pollutants at different pH values is similar to another study reported in the literature [39].

3.3. Contact Time Effect on the Adsorption

The adsorption of MO and Cr (VI) over polypyrrole@magnetic chitosan nanocomposite was performed at different reaction times ranging from 0 to 300 min as shown in Figure 4b. The adsorption investigations to study the contact-time effect were performed at 25 °C, pH 4.5, agitation speed 200 rpm, and adsorbent dosage 100 mg with initial pollutant concentrations of 100 mg/L. During the initial stage as shown in Figure 4b, there was rapid adsorption efficiency of MO and Cr (VI). The synergistic effects between adsorbate and adsorbent in the aqueous solution were responsible for a clear high adsorption efficiency.

This stage is the saturation phase in which all possible adsorption sites are saturated with the pollutants. In the case of the present adsorbent, saturation was achieved after 40 min due the interaction between adsorbent surface sites and the adsorbate ions. After the saturation phase, there was no substantial change. Thus, the adsorption of MO and Cr (VI) over the nanoadsorbent polypyrrole@magnetic chitosan is related to the physicochemical interactions between the adsorbate and adsorbent in water. Particle diffusion and mass transfer indicate that this system is chemically rate controlled.

3.4. Competitive Ions Effect

The selectivity of any promising adsorbent must be studied for different competing co-ions. Therefore, we studied the adsorption efficiency of polypyrrole@magnetic chitosan nanocomposite toward Cr (VI) and MO in the presence of bicarbonate, sulfate, and chloride co-ions, which may be present in drinking water (Figure 5a). These co-existing ions usually competed with the pollutants on the adsorption active sites over the polypyrrole@magnetic chitosan nanocomposite surface. To study the effect of co-ions, the adsorption experiment was performed at 25 °C, pH 4.5, agitation speed 200 rpm, contact time 40 m, and adsorbent dose 100 mg, with co-ion concentrations of 200 mg/L.

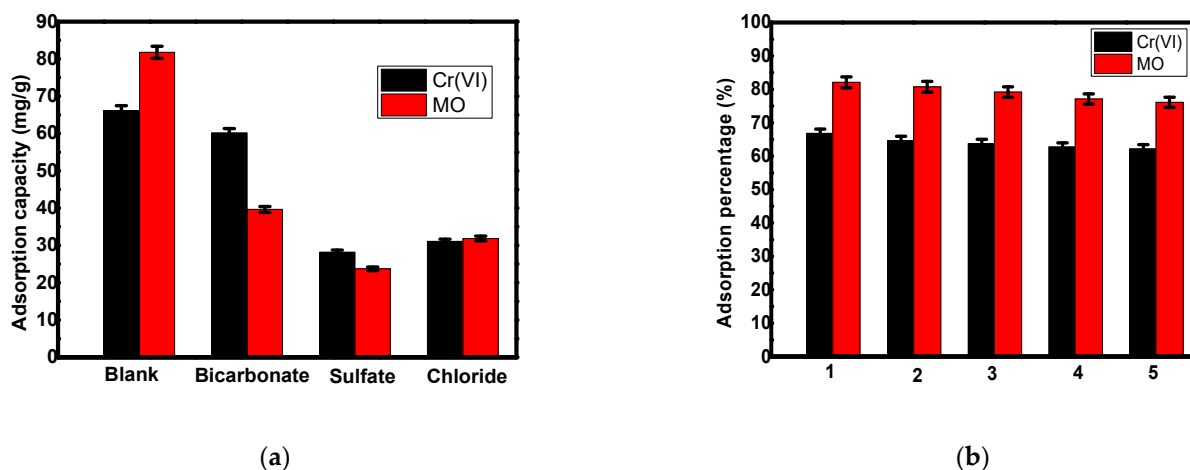


Figure 5. (a) Competitive ions effect on Cr (VI) and MO adsorption over polypyrrole@magnetic chitosan, and (b) reusability study of the nanocomposite toward Cr (VI) and MO adsorption from water.

According to Figure 5a, among the tested ions, sulphate showed the greatest effect for adsorption efficiency. This may be related to the higher affinity of the adsorbent amino group for SO_4^{2-} , which has higher electronic charge. On the other hand, chloride allowed an important reduction in the removal efficiency of both MO and Cr (VI). This may be attributed to their greater negative density charge compared to other negative ions. The similarity of ionic charge between Cr (VI) and bicarbonate ions had a greatly competitive effect on Cr(VI) adsorption [40]. In contrast, MO adsorption was not significantly affected by the bicarbonate ions.

3.5. Reusability of the Adsorbent

Reusability of any adsorbent is the main factor determining its economic feasibility for application in real water treatment. In order to study the reusability of polypyrrole@magnetic chitosan nanocomposite for the removal of both MO and Cr (VI), 5 successive cycles were performed using adsorbent dose of 100 mg in an adsorption–desorption experiment as shown in Figure 5b. During the desorption process, we applied 0.1 M sodium hydroxide as eluent. According to the Figure 5b, there was a little decrease in removal efficacy after each cycle. This decrease was attributed to the damage of the polypyrrole@magnetic chitosan nanocomposite reactive groups on the surface as well as to the loss of its integrity. Consequently, the excellent polypyrrole@magnetic chitosan nanocomposite

performance and reusability was approved for water treatment of MO and Cr (VI) after 5 regeneration cycles.

3.6. Adsorption Isotherm

The adsorption isotherm experiments were done to calculate the maximum adsorption efficiency of a polypyrrole@magnetic chitosan nanocomposite on MO and Cr (VI). The experiments were performed at 25 °C, pH 5.4, agitation speed 200 rpm, and adsorbent dosage 100 mg with initial MO and Cr (VI) concentrations ranging from 20 to 200 mg/L. Freundlich and Langmuir isotherms were used to study the relation between the initial concentration and the adsorption isotherm according to the following two equations, respectively.

$$C_e/q_e = (1/q_m^b) + (C_e/q_m), \quad (2)$$

$$\log q_e = \log K_F + 1/n(\log C_e), \quad (3)$$

where n and K_F are isotherm constants of the adsorption efficacy; b is the equilibrium constant; and q_m denotes maximum MO and Cr (VI) adsorption. Isotherm parameters here were calculated using Langmuir and Freundlich isotherms and tabulated in Table 1. The results are shown in Figure 6.

Table 1. Freundlich and Langmuir isotherm parameters for the removal of MO and Cr (VI) using polypyrrole@magnetic chitosan nanocomposite.

Pollutant	Freundlich					Langmuir			
	q_e (mg/g)	q_m (mg/g)	K_F (L·mg/g)	n	R^2	q_e (mg/g)	q_m (mg/g)	K_L (L·mg/g)	R^2
MO	88.8	97.9	46.9	4.789	0.880	94.9	97.9	0.323	0.998
Cr (VI)	101.5	106.4	32.7	4.679	0.847	104.8	106.4	0.268	0.997

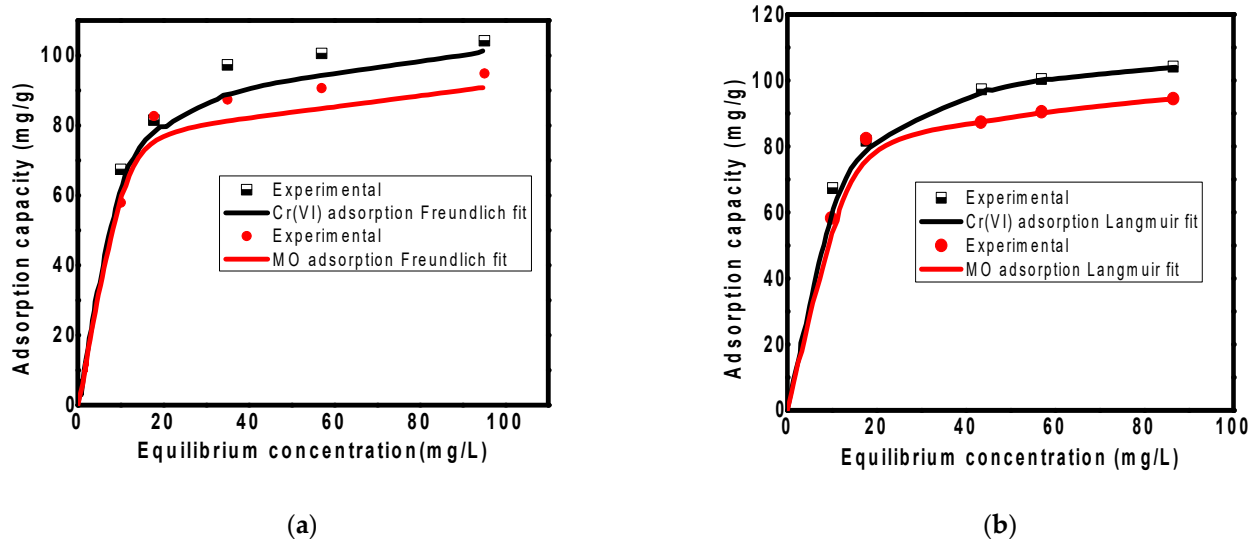


Figure 6. (a) Freundlich isotherm, and (b) Langmuir isotherm for the removal of MO and Cr(VI) over polypyrrole@magnetic chitosan nanocomposite.

Homogeneous adsorption sites and monolayer interaction between the nanocomposite surface and adsorbates (MO, Cr (VI)) were confirmed from the regression coefficient (R^2), which indicated that the Langmuir isotherm was more fit than the Freundlich isotherm as shown in Table 1. This was an indication of the behavior of the nanocomposite adsorption monolayer besides active sites homogeneity. Also, it showed that the different active sites on the nanocomposite surface have energetically equivalent properties. According to this, the chemical bonds between the adsorbent and adsorbates primarily showed monolayer

adsorption over the studied nanoadsorbent with no additional interaction between the adsorbed pollutant molecules and other pollutants. Interestingly, the MO and Cr (VI) maximum removal capacity over the polypyrrole@magnetic chitosan nanocomposite was found to be 95 and 105 mg/g, respectively, which is higher than previous reported studies as tabulated in Table 2.

Table 2. The comparison between the removal of MO and Cr (VI) over polypyrrole@magnetic chitosan nanocomposite and previous studies.

Adsorbent	Operating Conditions	Removal Efficiency (mg/g)		Ref.
		MO	Cr (VI)	
ppy@magnetic chitosan	dosage: 100 mg/L, contact time: 40 min, 25 °C; 200 rpm, pH 4.5	95	105	This study
Magnetic biochar	dosage: 200 mg/L; contact time: 5 days, 25 °C, 160 rpm, pH 5	-	77.54	[41]
Chitosan/diatomite composite	dosage: 0.2 g/L, contact time: 40 min, 25 °C, pH 5	35	-	[42]
CuO NPs Graphene oxide	dosage: 25 mg/L, contact time: 100 min, 25–40 °C, pH 3	-	16.83	[37]
Banana peel	dosage: 100 mg/L, contact time: 24 h, 30 °C, 180 rpm, pH 6–7	21	-	[43]
Cetylpyridinium bromide modified Montmorillonite	Dosage: 50 mg/L, contact time: 60 min, 25 °C, 150 rpm, pH 4	6.54	-	[44]
Modified wheat straw Hydrotalcite	Dosage: 5–10 mg/L; contact time: 24 h, 30 °C, 250 rpm, pH 6	-	17	[45]
Hydrotalcite sepiolite-supported nanoscale zero-valent iron (S-NZVI)	Dosage: 0.05–3.2 g/L contact time: 11 min, 28 °C, 200 rpm, pH 6		43.86	[23]
TiO ₂ @MIL-101 core-shell	Dosage: 150 mg/L contact time: 4 h	19.23	-	[46]
Chitosan/alumina composite	Dosage: 10 mg/L contact time: 60 min, 303 °C, 200 rpm, pH 4	-	6.127	[47]
Nano-hydrotalcite SiO ₂ composite	Dosage: 1 g/L contact time: 24 h	35	-	[48]
Chitosan/organic rectorite-Fe ₃ O ₄	Dosage: 40 mg/L contact time: 80 min, 25 °C, 200 rpm, pH 3	5.56		[49]

3.7. Adsorption Mechanism

FT-IR and XPS investigations were used to study the composition of ppy@magnetic chitosan before and after the adsorption of MO and Cr (VI) to determine the mechanisms of pollutant removal. FT-IR of ppy@magnetic chitosan nanocomposite before and after adsorption of MO and Cr (VI) is shown in Figure 7a. The MO characteristic stretching bands corresponding to C–C, C–N, S=O, and C–H appear at 1607, 1369, 1121, and 826 cm⁻¹ [50] in FT-IR results of ppy@magnetic chitosan adsorbed MO. The slight displacement of bands from their locations was likely observed in FT-IR of ppy@magnetic chitosan adsorbed Cr (VI). In order to approve these results, full range XPS before and after the adsorption of target pollutants was used to identify the adsorbed species over the adsorbent as shown in Figure 7b. The MO and Cr (VI) characteristic peaks appeared as shown in Figure 7b, indicating the effective accumulation of Cr (VI) and MO over the adsorbent surface through the adsorption process.

Furthermore, the XPS spectrum was used to identify the adsorbed species of chromium ions (Figure 8a). XPS analysis showed two satellite bands of Cr (VI) and Cr (III) that appear at 577 and 587 eV, respectively.

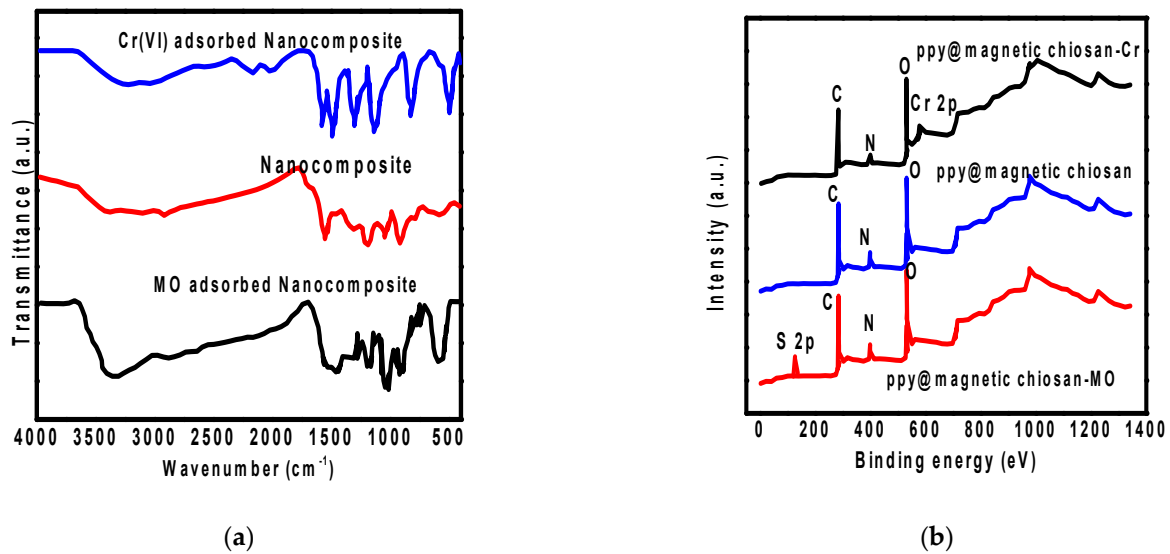


Figure 7. (a) FT-IR and (b) full range XPS spectrum of ppy@magnetic chitosan before and after Cr (VI) and MO adsorption.

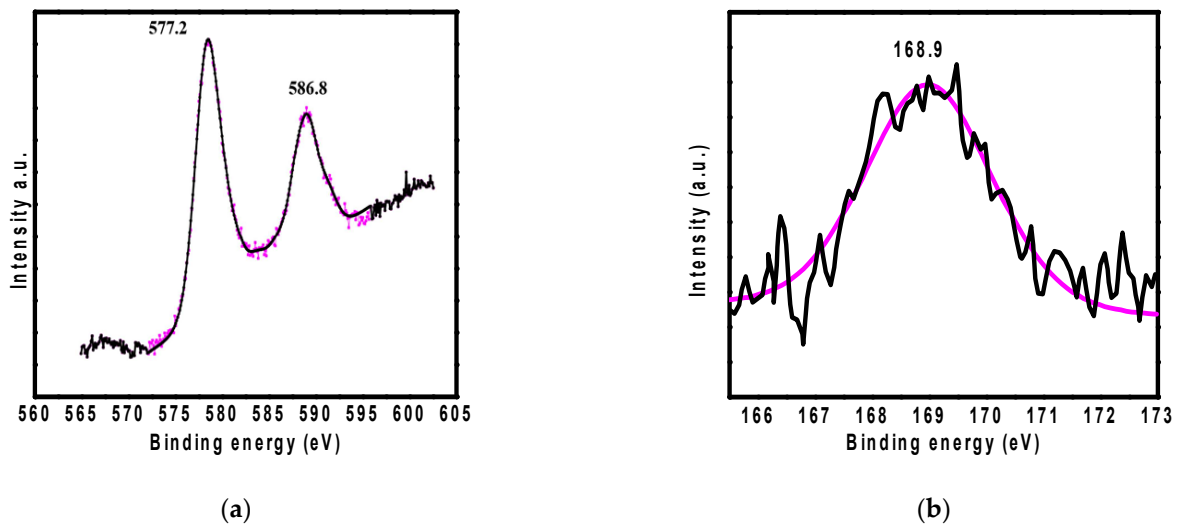


Figure 8. XPS spectra of ppy@magnetic chitosan after Cr (VI) adsorption (a) and MO adsorption (b).

These results suggested that Cr (III) ions are present as chromium species over the surface of the adsorbent. Additionally, the existence of satellite bands of both Cr (VI) and Cr (III) confirmed the adsorption of Cr (VI) over ppy@magnetic chitosan besides the chemical reduction of Cr (VI) to Cr (III) during the adsorption. Subsequently, the chromium removing mechanism can be explained as follows: under acidic conditions, the NH-functional groups were protonated followed by the adsorption of Cr (VI) species (HCrO_4^-) over the adsorbent via bonding with nitrogen species and via electrostatic interactions.

This chemical bonding associated with the oxidation of -NH- to =N- was subsequently accompanied by the reduction of hexavalent chromium to Cr (III). The redox activity of =N-/-NH- pairs is responsible for the reduction of Cr (VI) in addition to their minor oxidation potential compared to the Cr (III)/Cr (VI) redox pair. In addition, few Cr (III) species may be dissolved in water, and others could be removed via complexation with ppy@magnetic chitosan nitrogen functional groups. On the other hand, the XPS spectrum of ppy@magnetic chitosan after the adsorption of MO showed a satellite peak at 169 eV, which indicated the adsorption of MO over the binding sites of the nanocomposite. In general, the redox activity of ppy@magnetic chitosan, besides the existence of different functional groups over its surface, gave the adsorbent amazing in situ chemical reduction properties

and adsorption toward Cr (VI) and MO removal from aqueous solution. Consequently, this innovative adsorbent could be used for water detoxification from pollutants.

4. Conclusions

In this study, a novel ppy@magnetic chitosan nanocomposite was synthesized. This novel adsorbent contained magnetic Fe₃O₄ nanoparticles and several N-containing functional groups giving it an effective application for water detoxification from both MO and Cr (VI). This nanocomposite was successfully characterized using different techniques including SEM, TEM, TGA XRD, and FT-IR. The effect of different factors on the adsorption of MO and Cr (VI) over the synthesized nanocomposite was studied, including contact time, pH, and co-existed ions. The study of the contact time effect indicated that the adsorption system was chemically rate-controlled. The pH effect study revealed that MO and Cr (VI) adsorption over the studied adsorbent was pH dependent and more suitable for an acidic environment at pH between 2 and 4.5. The study of the co-existing ions effect revealed that the most affected co-ion on adsorption efficiency was sulfate, while bicarbonate had the lowest effect. The adsorption isotherm suggested monolayer adsorption of MO and Cr (VI) over a polymeric-inorganic nanocomposite due to its good fit with the Langmuir isotherm. MO and Cr (VI) maximal removal efficiencies over this magnetic polymer nanocomposite reached 95 and 105 mg/g, respectively. The reusability study using 0.1 M NaOH as eluent also indicated an excellent reusability of the nanocomposite up to 5 successive cycles with a slight reduction in the removal efficiency toward MO and Cr (VI), which was attributed to the loss of functional group activity. FT-IR and XPS studies approved the successful adsorption of both MO and Cr (VI) over the adsorbent surface in addition to the reduction of Cr (VI) to Cr (III). Finally, we can conclude that ppy@magnetic chitosan nanocomposite is a promising adsorbent for removing MO and Cr (VI) from water.

Author Contributions: Conceptualization A.A., N.S.A., K.M.K., F.M.A., M.A.T., and F.B.R.; methodology A.A., N.S.A., K.M.K., F.M.A., M.A.T. and F.B.R.; formal analysis; data curation A.A., N.S.A., K.M.K., F.M.A., M.A.T., and F.B.R.; Writing—original draft preparation, A.A., N.S.A., K.M.K., F.M.A., and M.A.T.; writing—review and editing, A.A., N.S.A., K.M.K., F.M.A., M.A.T., and F.B.R.; visualization; F.B.R. All authors have read and agreed to the published version of the manuscript.

Funding: This research was funded by Deanship of Scientific Research at King Khalid University.

Institutional Review Board Statement: Not applicable.

Informed Consent Statement: Not applicable.

Data Availability Statement: Data sharing is not applicable.

Acknowledgments: The authors extend their appreciation to the Deanship of Scientific Research at King Khalid University for funding this work through research groups program under grant number R.G.P2/157/42. Also, this research was funded by the Deanship of Scientific Research at Princess Nourah bint Abdulrahman University through the Fast-track Research Funding Program.

Conflicts of Interest: The authors declare no conflict of interest.

References

1. Tagoon, M.A.; Siddeeg, S.M.; Salem Alsaiani, N.; Mnif, W.; Ben Rebah, F. Effective heavy metals removal from water using nanomaterials: A review. *Processes* **2020**, *8*, 645. [[CrossRef](#)]
2. Siddeeg, S.M.; Tagoon, M.A.; Ben Rebah, F. Agro-industrial waste materials and wastewater as growth media for microbial biofloculants production: A review. *Mater. Res. Express* **2019**, *7*, 012001. [[CrossRef](#)]
3. Siddeeg, S.M.; Tagoon, M.A.; Alsaiani, N.S.; Shabbir, M.; Ben Rebah, F. Application of Functionalized Nanomaterials as Effective Adsorbents for the Removal of Heavy Metals from Wastewater: A Review. *Curr. Anal. Chem.* **2021**, *17*, 4–22. [[CrossRef](#)]
4. Li, K.; Miwornunyuie, N.; Chen, L.; Jingyu, H.; Amaniampong, P.S.; Ato Koomson, D.; Ewusi-Mensah, D.; Xue, W.; Li, G.; Lu, H. Sustainable Application of ZIF-8 for Heavy-Metal Removal in Aqueous Solutions. *Sustainability* **2021**, *13*, 984. [[CrossRef](#)]
5. Mohd Makhtar, N.S.; Idris, J.; Musa, M.; Andou, Y.; Ku Hamid, K.H.; Puasa, S.W. Plant-Based *Tacca leontopetaloides* Biopolymer Flocculant (TBPF) Produced High Removal of Heavy Metal Ions at Low Dosage. *Processes* **2021**, *9*, 37. [[CrossRef](#)]
6. Khalil, U.; Shakoor, M.B.; Ali, S.; Ahmad, S.R.; Rizwan, M.; Alsahli, A.A.; Alyemeni, M.N. Selective Removal of Hexavalent Chromium from Wastewater by Rice Husk: Kinetic, Isotherm and Spectroscopic Investigation. *Water* **2021**, *13*, 263. [[CrossRef](#)]

7. Campisi, S.; Evangelisti, C.; Postole, G.; Gervasini, A. Combination of interfacial reduction of hexavalent chromium and trivalent chromium immobilization on tin-functionalized hydroxyapatite materials. *Appl. Surf. Sci.* **2021**, *539*, 148227. [[CrossRef](#)]
8. Athira, T.; Roshith, M.; Babu, T.S.; Kumar, D.V.R. Fibrous red phosphorus as a non-metallic photocatalyst for the effective reduction of Cr (VI) under direct sunlight. *Mater. Lett.* **2021**, *283*, 128750. [[CrossRef](#)]
9. WHO. *Guidelines for Drinking Water Quality*, 4th ed.; WHO: Geneva, Switzerland, 2011.
10. Mystrioti, C.; Koursari, S.; Xenidis, A.; Papassiopi, N. Hexavalent Chromium Reduction by Gallic Acid. *Chemosphere* **2021**, *273*, 129737. [[CrossRef](#)] [[PubMed](#)]
11. Ihlenburg, R.B.; Lehnen, A.-C.; Koetz, J.; Taubert, A. Sulfobetaine Cryogels for Preferential Adsorption of Methyl Orange from Mixed Dye Solutions. *Polymers* **2021**, *13*, 208. [[CrossRef](#)]
12. Li, Y.; Deng, M.; Wang, X.; Wang, Y.; Li, J.; Xia, S.; Zhao, J. In-situ remediation of oxytetracycline and Cr (VI) co-contaminated soil and groundwater by using blast furnace slag-supported nanosized Fe⁰/Fe_x. *Chem. Eng. J.* **2021**, *412*, 128706. [[CrossRef](#)]
13. Stern, C.M.; Jegede, T.O.; Hulse, V.A.; Elgrishi, N. Electrochemical reduction of Cr (VI) in water: Lessons learned from fundamental studies and applications. *Chem. Soc. Rev.* **2021**, *50*, 1642–1667. [[CrossRef](#)] [[PubMed](#)]
14. Sabri, M.A.; Sara, Z.; Al-Sayah, M.H.; Ibrahim, T.H.; Khamis, M.I.; El-Kadri, O.M. Simultaneous Adsorption and Reduction of Cr (VI) to Cr (III) in Aqueous Solution Using Nitrogen-Rich Amino-Linked Porous Organic Polymers. *Sustainability* **2021**, *13*, 923. [[CrossRef](#)]
15. Gallo-Cordova, A.; Lemus, J.; Palomares, F.J.; Morales, M.; Mazarío, E. Superparamagnetic nanosorbent for water purification: Assessment of the adsorptive removal of lead and methyl orange from aqueous solutions. *Sci. Total Environ.* **2020**, *711*, 134644. [[CrossRef](#)] [[PubMed](#)]
16. Niazi, L.; Lashanizadegan, A.; Sharififard, H. Chestnut oak shells activated carbon: Preparation, characterization and application for Cr (VI) removal from dilute aqueous solutions. *J. Clean. Prod.* **2018**, *185*, 554–561. [[CrossRef](#)]
17. Liu, J.; Zhou, Q.; Chen, J.; Zhang, L.; Chang, N. Phosphate adsorption on hydroxyl-iron-lanthanum doped activated carbon fiber. *Chem. Eng. J.* **2013**, *215*, 859–867. [[CrossRef](#)]
18. Kumar, N.; Reddy, L.; Parashar, V.; Ngila, J.C. Controlled synthesis of microsheets of ZnAl layered double hydroxides hexagonal nanoplates for efficient removal of Cr (VI) ions and anionic dye from water. *J. Environ. Chem. Eng.* **2017**, *5*, 1718–1731. [[CrossRef](#)]
19. Karthikeyan, P.; Banu, H.A.T.; Meenakshi, S. Removal of phosphate and nitrate ions from aqueous solution using La³⁺ incorporated chitosan biopolymeric matrix membrane. *Int. J. Biol. Macromol.* **2019**, *124*, 492–504. [[CrossRef](#)]
20. Anbinder, P.S.; Macchi, C.; Amalvy, J.; Somoza, A. A study of the structural changes in a chitosan matrix produced by the adsorption of copper and chromium ions. *Carbohydr. Polym.* **2019**, *222*, 114987. [[CrossRef](#)]
21. Kaur, M.; Kaur, N.; Jeet, K.; Kaur, P. MgFe₂O₄ nanoparticles loaded on activated charcoal for effective removal of Cr (VI)—A novel approach. *Ceram. Int.* **2015**, *41*, 13739–13750. [[CrossRef](#)]
22. Yang, Y.; Yang, J.; Du, Y.; Li, C.; Wei, K.; Lu, J.; Chen, W.; Yang, L. Preparation and Characterization of Cationic Water-Soluble Pillar [5] arene-Modified Zeolite for Adsorption of Methyl Orange. *ACS Omega* **2019**, *4*, 17741–17751. [[CrossRef](#)]
23. Fu, R.; Yang, Y.; Xu, Z.; Zhang, X.; Guo, X.; Bi, D. The removal of chromium (VI) and lead (II) from groundwater using sepiolite-supported nanoscale zero-valent iron (S-NZVI). *Chemosphere* **2015**, *138*, 726–734. [[CrossRef](#)]
24. Chen, P.; Xie, F.; Tang, F.; McNally, T. Influence of plasticiser type and nanoclay on the properties of chitosan-based materials. *Eur. Polym. J.* **2021**, *144*, 110225. [[CrossRef](#)]
25. Fan, S.; Liu, Z.; Wu, Y.; Zhang, Y.; Hu, H.; Huang, Z.; Qin, Y.; Liang, J. 3D porous tubular network-structured chitosan-based beads with multifunctional groups: Highly efficient and selective removal of Cu²⁺. *Int. J. Biol. Macromol.* **2021**, *171*, 17–27. [[CrossRef](#)] [[PubMed](#)]
26. Saravanan, A.; Kumar, P.S.; Govarthanan, M.; George, C.S.; Vaishnavi, S.; Mouliswaran, B.; Kumar, S.P.; Jeevanantham, S.; Yaashikaa, P. Adsorption characteristics of magnetic nanoparticles coated mixed fungal biomass for toxic Cr (VI) ions in aquatic environment. *Chemosphere* **2021**, *267*, 129226. [[CrossRef](#)] [[PubMed](#)]
27. Zeng, H.; Zhai, L.; Zhang, J.; Li, D. As (V) adsorption by a novel core-shell magnetic nanoparticles prepared with Iron-containing water treatment residuals. *Sci. Total Environ.* **2021**, *753*, 142002. [[CrossRef](#)]
28. Qiu, X.; Wang, S.; Miao, S.; Suo, H.; Xu, H.; Hu, Y. Co-immobilization of laccase and ABTS onto amino-functionalized ionic liquid-modified magnetic chitosan nanoparticles for pollutants removal. *J. Hazard. Mater.* **2021**, *401*, 123353. [[CrossRef](#)]
29. Ren, Y.; Abbood, H.A.; He, F.; Peng, H.; Huang, K. Magnetic EDTA-modified chitosan/SiO₂/Fe₃O₄ adsorbent: Preparation, characterization, and application in heavy metal adsorption. *Chem. Eng. J.* **2013**, *226*, 300–311. [[CrossRef](#)]
30. Wang, J.; Pan, K.; He, Q.; Cao, B. Polyacrylonitrile/polypyrrole core/shell nanofiber mat for the removal of hexavalent chromium from aqueous solution. *J. Hazard. Mater.* **2013**, *244*, 121–129. [[CrossRef](#)]
31. Siddeeg, S.M.; Tahoon, M.A.; Mnif, W.; Ben Rebah, F. Iron oxide/chitosan magnetic nanocomposite immobilized manganese peroxidase for decolorization of textile wastewater. *Processes* **2020**, *8*, 5. [[CrossRef](#)]
32. Yuvaraj, H.; Woo, M.H.; Park, E.J.; Jeong, Y.T.; Lim, K.T. Polypyrrole/γ-Fe₂O₃ magnetic nanocomposites synthesized in supercritical fluid. *Eur. Polym. J.* **2008**, *44*, 637–644. [[CrossRef](#)]
33. Govindan, S.; Nivethaa, E.; Saravanan, R.; Narayanan, V.; Stephen, A. Synthesis and characterization of chitosan–silver nanocomposite. *Appl. Nanosci.* **2012**, *2*, 299–303. [[CrossRef](#)]
34. M Siddeeg, S.; A Tahoon, M.; Ben Rebah, F. Simultaneous Removal of Calconcarboxylic Acid, NH₄⁺ and PO₄³⁻ from Pharmaceutical Effluent Using Iron Oxide-Biochar Nanocomposite Loaded with *Pseudomonas putida*. *Processes* **2019**, *7*, 800. [[CrossRef](#)]

35. Siddeeg, S.M.; Amari, A.; Tahoona, M.A.; Alsaiani, N.S.; Ben Rebah, F. Removal of meloxicam, piroxicam and Cd²⁺ by Fe₃O₄/SiO₂/glycidyl methacrylate-S-SH nanocomposite loaded with laccase. *Alex. Eng. J.* **2020**, *59*, 905–914. [[CrossRef](#)]
36. Bhaumik, M.; Maity, A.; Srinivasu, V.; Onyango, M.S. Enhanced removal of Cr (VI) from aqueous solution using polypyrrole/Fe₃O₄ magnetic nanocomposite. *J. Hazard. Mater.* **2011**, *190*, 381–390. [[CrossRef](#)]
37. Robati, D.; Mirza, B.; Rajabi, M.; Moradi, O.; Tyagi, I.; Agarwal, S.; Gupta, V. Removal of hazardous dyes-BR 12 and methyl orange using graphene oxide as an adsorbent from aqueous phase. *Chem. Eng. J.* **2016**, *284*, 687–697. [[CrossRef](#)]
38. Li, K.; Li, P.; Cai, J.; Xiao, S.; Yang, H.; Li, A. Efficient adsorption of both methyl orange and chromium from their aqueous mixtures using a quaternary ammonium salt modified chitosan magnetic composite adsorbent. *Chemosphere* **2016**, *154*, 310–318. [[CrossRef](#)] [[PubMed](#)]
39. Chen, S.; Huang, Y.; Han, X.; Wu, Z.; Lai, C.; Wang, J.; Deng, Q.; Zeng, Z.; Deng, S. Simultaneous and efficient removal of Cr (VI) and methyl orange on LDHs decorated porous carbons. *Chem. Eng. J.* **2018**, *352*, 306–315. [[CrossRef](#)]
40. Karthikeyan, P.; Elanchezhian, S.S.; Preethi, J.; Meenakshi, S.; Park, C.M. Mechanistic performance of polyaniline-substituted hexagonal boron nitride composite as a highly efficient adsorbent for the removal of phosphate, nitrate, and hexavalent chromium ions from an aqueous environment. *Appl. Surf. Sci.* **2020**, *511*, 145543. [[CrossRef](#)]
41. Han, Y.; Cao, X.; Ouyang, X.; Sohi, S.P.; Chen, J. Adsorption kinetics of magnetic biochar derived from peanut hull on removal of Cr (VI) from aqueous solution: Effects of production conditions and particle size. *Chemosphere* **2016**, *145*, 336–341. [[CrossRef](#)]
42. Zhao, P.; Zhang, R.; Wang, J. Adsorption of methyl orange from aqueous solution using chitosan/diatomite composite. *Water Sci. Technol.* **2017**, *75*, 1633–1642. [[CrossRef](#)]
43. Annadurai, G.; Juang, R.-S.; Lee, D.-J. Use of cellulose-based wastes for adsorption of dyes from aqueous solutions. *J. Hazard. Mater.* **2002**, *92*, 263–274. [[CrossRef](#)]
44. Hu, B.; Luo, H. Adsorption of hexavalent chromium onto montmorillonite modified with hydroxyaluminum and cetyltrimethylammonium bromide. *Appl. Surf. Sci.* **2010**, *257*, 769–775. [[CrossRef](#)]
45. Lazaridis, N.; Pandi, T.; Matis, K. Chromium (VI) removal from aqueous solutions by Mg–Al–CO₃ hydrotalcite: Sorption–desorption kinetic and equilibrium studies. *Ind. Eng. Chem. Res.* **2004**, *43*, 2209–2215. [[CrossRef](#)]
46. Chang, N.; Zhang, H.; Shi, M.-S.; Li, J.; Shao, W.; Wang, H.-T. Metal-organic framework templated synthesis of TiO₂@MIL-101 core-shell architectures for high-efficiency adsorption and photocatalysis. *Mater. Lett.* **2017**, *200*, 55–58. [[CrossRef](#)]
47. Gandhi, M.R.; Meenakshi, S. Preparation and characterization of La (III) encapsulated silica gel/chitosan composite and its metal uptake studies. *J. Hazard. Mater.* **2012**, *203*, 29–37. [[CrossRef](#)] [[PubMed](#)]
48. Pérez, E.; Ayele, L.; Getachew, G.; Fetter, G.; Bosch, P.; Mayoral, A.; Díaz, I. Removal of chromium (VI) using nano-hydrotalcite/SiO₂ composite. *J. Environ. Chem. Eng.* **2015**, *3*, 1555–1561. [[CrossRef](#)]
49. Zeng, L.; Xie, M.; Zhang, Q.; Kang, Y.; Guo, X.; Xiao, H.; Peng, Y.; Luo, J. Chitosan/organic rectorite composite for the magnetic uptake of methylene blue and methyl orange. *Carbohydr. Polym.* **2015**, *123*, 89–98. [[CrossRef](#)]
50. Deng, L.; Shi, Z.; Peng, X.; Zhou, S. Magnetic calcinated cobalt ferrite/magnesium aluminum hydrotalcite composite for enhanced adsorption of methyl orange. *J. Alloys Compd.* **2016**, *688*, 101–112. [[CrossRef](#)]